Multi-Objective Design Optimization of a Variable Geometry Spray Fuel Injector

J. R. Archer
Graduate Research Assistant
North Carolina State University,
Raleigh, NC 27695
e-mail: jrarcher@ncsu.edu

Tiegang Fang
Associate Professor
North Carolina State University,
Raleigh, NC 27695
e-mail: tfang2@ncsu.edu

Scott Ferguson[1]
Assistant Professor
North Carolina State University,
Raleigh, NC 27695
e-mail: scott_ferguson@ncsu.edu

Gregory D. Buckner
Professor
North Carolina State University,
Raleigh, NC 27695
e-mail: gdbucker@ncsu.edu

This paper explores the simulation-based design optimization of a variable geometry spray (VGS) fuel injector. A multi-objective genetic algorithm (MOGA) is interfaced with commercial computational fluid dynamics (CFD) software and high performance computing capabilities to evaluate the spray characteristics of each VGS candidate design. A three-point full factorial experimental design is conducted to identify significant design variables and to better understand possible variable interactions. The Pareto frontier of optimal designs reveals the inherent tradeoff between two performance objectives—actuator stroke and spray angle sensitivity. Analysis of these solutions provides insight into dependencies between design parameters and the performance objectives and is used to assess possible performance gains with respect to initial prototype configurations. These insights provide valuable design information for the continued development of this VGS technology. [DOI: 10.1115/1.4026263]

1 Introduction

Designers of internal combustion (IC) engines are required to meet increasingly strict regulations on emissions. The US Environmental Protection Agency [1], for example, has set maximum levels for particulate matter and nitrogen oxides that are difficult to meet using conventional diesel combustion methods. Homogeneous charge compression ignition (HCCI) is one promising solution [2], but it uses a lean mixture to minimize soot formation that produces lower power densities than conventional diesel combustion [3]. While dual-mode combustion strategies have been proposed using HCCI [4–6], conventional fuel injectors have fixed spray geometries that are suboptimal for all modes [7].

Variable-geometry spray (VGS) fuel injection may address this need by enabling independent control of fuel flow rate and spray geometry. By optimizing air-fuel mixing and the distribution of atomized fuel within the cylinder, VGS injection has the potential to maximize power output by enabling combustion at peak efficiency. Prior work by the authors generated three VGS fuel injector prototypes [8] that continuously control the fuel spray angle independent of fuel flow rate or other vital injection parameters. However, each concept required approximately 25,000 man-hours for design, fabrication and experimental evaluation, leaving most of the design space unexplored.

This paper explores the simulation-based design optimization of a hollow-cone VGS injector used in diesel internal combustion engines. Design space exploration is enabled by a multiobjective genetic algorithm (MOGA), interfaces between advanced simulation engines, and high performance computing. Regression analysis is used to understand what design parameters have the greatest influence on system performance and estimates of the optimal performance frontier are compared against theoretical limits.

2 Background

While pintle mechanisms have been used in conventional fuel injectors to regulate fuel flow [9], this work explores a VGS design capable of varying fuel spray angle. The VGS is centrally positioned and the optimal spray angle targets the lip of the piston bowl throughout the compression stroke to minimize liner wetting and fuel impingement. As shown in Fig. 1, when the pintle is fully retracted into the nozzle, the spray cone has a narrow included angle; when fully deployed this angle is significantly increased. By manipulating the position of this pintle relative to the nozzle orifice, a wide and controllable range of spray angles can be achieved [10].

Prior research has shown that optimal spray angle trajectory can plotted as a function of engine timing [11]. Experimental validation of spray angle variation (70–150 deg) by manipulating pintle position was achieved using a low-pressure prototype with a 200 μm annular gap between the nozzle and pintle. Using pressurized water (200–1500 psi), spray angles were measured using digital image postprocessing for 13 pintle positions and four operating pressures [11]. While this prototype demonstrated repeatable spray angle control using pintle displacement, limitations included manual actuation, dimensions that did not conform to conventional rail fuel injectors, a spray range that was not consistent with design requirements (2–93 deg), and a total pintle displacement that was larger than desired (750 μm). Further, the large annular gap and low operating pressures led to spray droplet sizes approximately five times larger than those of conventional injectors.

A second prototype was designed based on component measurements from conventional diesel injectors [12]; it featured a pintle diameter of 1.5 mm and an annular gap of 100 μm. External nozzle dimensions were chosen to be consistent with "P-type" common fuel injectors and manual actuation was replaced by a piezoceramic stack actuator with closed loop pintle displacement control. Experiments using water pressurized at 500 psi, 1000 psi, and 1500 psi demonstrated an increase in the range of spray angles achieved (12–140 deg) with reduced pintle displacement (450 μm) at bandwidths of up to 20 Hz [13]. Further, droplet size measurements were small enough to meet secondary design objectives [11].

Electronic regulation of working fluid flow in this prototype was achieved using a solenoid valve. However, when the solenoid was deactivated, a finite volume of working fluid remained in the channel between the solenoid and the injector nozzle. This fluid drained out of the injector at pressures and velocities so low that it did not atomize, resulting in unacceptable droplet formation. Conventional rail injectors minimize leakage using nozzle needles [14], which shut off the flow by blocking the injection holes as it is pressed against the needle seat. In its activated state, the nozzle needle is lifted up to allow fluid to flow out the injection holes. A

[1]Corresponding author.

Contributed by the Design Automation Committee of ASME for publication in the Journal of Mechanical Design. Manuscript received March 18, 2013; final manuscript received November 1, 2013; published online February 12, 2014. Assoc. Editor: Matthew B. Parkinson.

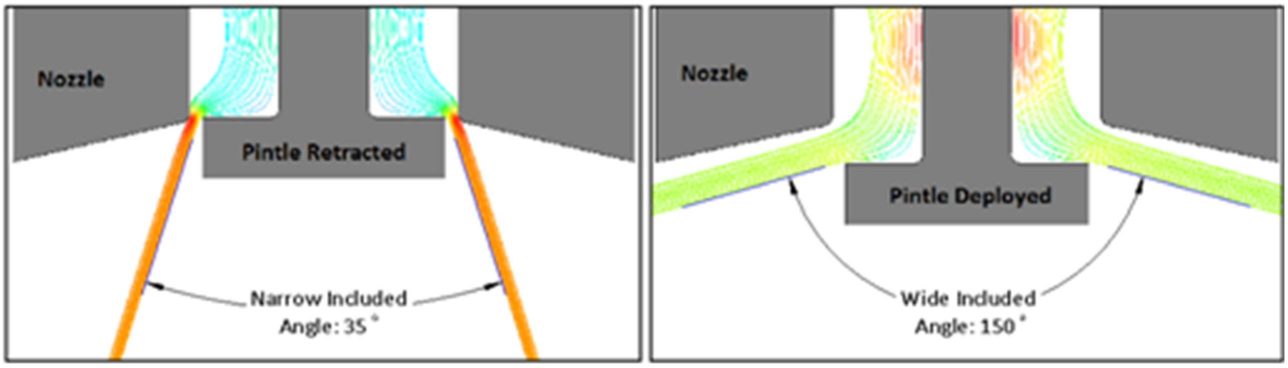

Fig. 1 2D simulation results of the VGS fuel injection concept

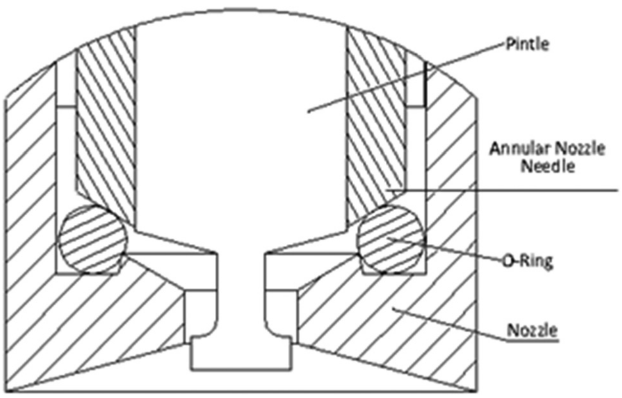

Fig. 2 Cross section of the distal portion of the third-generation VGS prototype

third generation prototype was then designed with an annular nozzle needle to accommodate the centrally located pintle, as shown in Fig. 2. This nozzle needle was electromechanically actuated in similar fashion to conventional rail injectors [14], yet due the limitations of fabrication processes, an O-ring was incorporated to seal the nozzle. This O-ring was not included in the model described in Sec. 3, mainly because its distance from the nozzle prevents it from significantly influencing the spray angle. Additionally, while initial experimental testing confirmed the reduction of postinjection fluid drainage, final production should replace the O-ring with two high tolerance metal surfaces.

3 Developing the Simulation Model

Three years of research and development produced only three functional VGS prototypes, none optimized for implementation in a real IC engine. Enabling a more complete exploration of the problem required simulation capabilities to accurately model fuel spray characteristics for specific flow conditions and pintle displacements. Computational fluid dynamics (CFD) packages provide this ability using sophisticated meshing algorithms that discretize the fuel flow regime into finite elements. ANSYS CFX [15] was chosen because of its ability to be run in batch mode with Python [16]. After comparing experimental data and simulation engine results, the homogeneous k-epsilon model was chosen. Simulation convergence was set to 100 iterations or when all residuals reached 1E-4. These limits were established after watching hundreds of runs converge during model development.

The two-dimensional axisymmetric model shown in Fig. 2 was used to exploit azimuthal symmetry of each candidate design. Unstructured, triangular meshes were employed to map the curved surfaces of the flow domain and maintain consistent element sizes [17]. A steady state, two-phase CFD analysis was performed on the flow domain, where the fluid volume initially contained only air at standard temperature and pressure. Because of its similarity

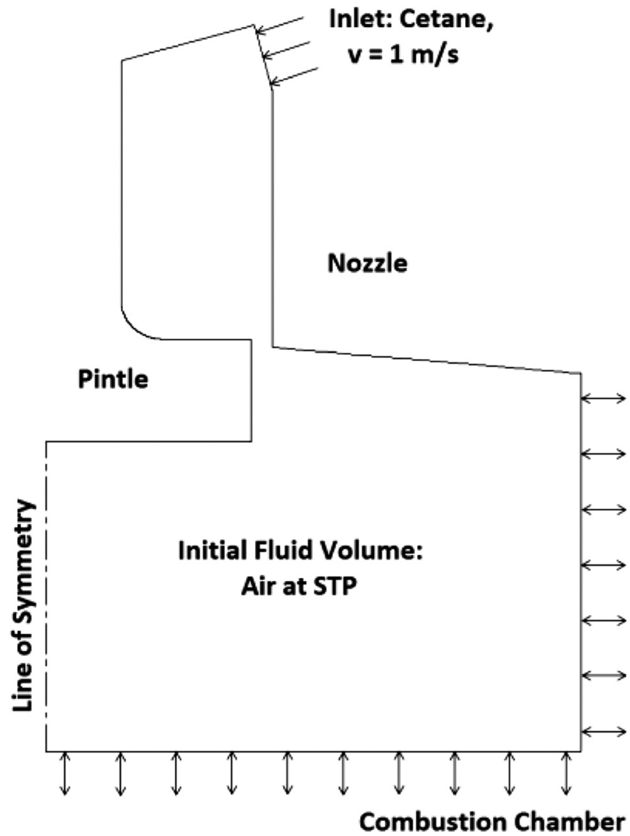

Fig. 3 2D axisymmetric model showing boundary conditions and domain initialization

to diesel fuel and use in fuel injection testing, Cetane ($C_{16}H_{34}$) with a unit volume fraction was used as the working fluid. The specified boundary conditions, shown in Fig. 3, established a fuel inlet velocity of 1 m/s, a relative combustion chamber pressure of zero, and defined all pintle and nozzle surfaces to be no-slip boundaries. Fuel pressures used in the CFD analysis were set to 14.5 psi because simulating with elevated operating pressures significantly increased the computational burden and experimentally measured spray angles using the prototypes had shown very little dependence on operating pressure [13].

For each candidate VGS design, nine CFD simulations were performed to quantify the relationship between spray angle and pintle position. These simulations covered a pintle displacement range of 0–400 μm. The included spray angle, θ, was estimated using Eq. (1); where x_p, y_p represent the coordinates of the interior corner of the pintle, and x_s, y_s represent the point where the streamlines exit the flow domain as shown in Fig. 4

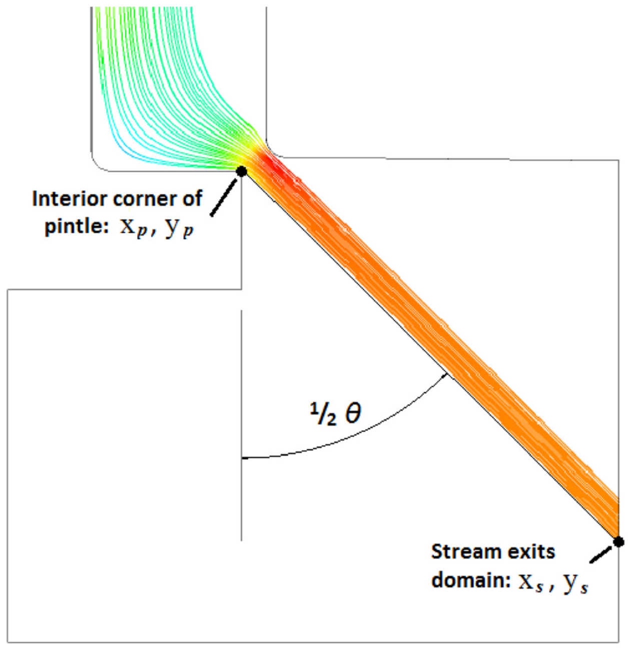

Fig. 4 CFD results showing the locations of x_p, y_p and x_s, y_s

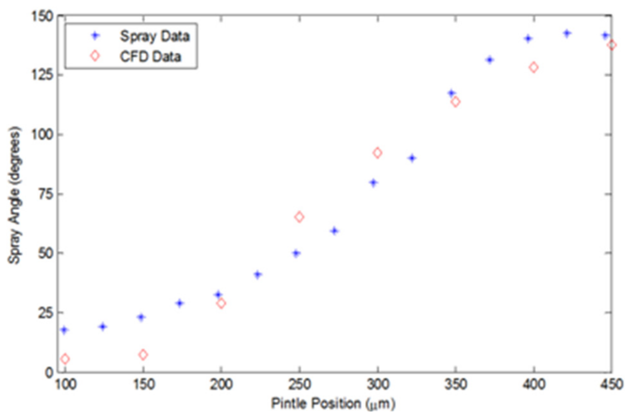

Fig. 5 Experimental validation of CFD model

$$\theta = 2 \cdot \tan^{-1}\left(\frac{x_s - x_p}{y_s - y_p}\right) \tag{1}$$

To address the tradeoff between computational burden and accuracy, initial simulations for a given design geometry and boundary condition were performed at a various mesh sizes. Simulations began with an extremely fine uniform mesh (10 μm), which was linearly increased to 160 μm. Attempts to refine the mesh around the pintle where the flow converged led to inaccurate results. A continually adaptive mesh was also tested but led to significant increases in convergence times. A uniform mesh size of 15 μm was finally selected because it reduced computational time by 50% (7 min as opposed to 14 min) while maintaining an average spray angle error of approximately 1 deg (total recorded range 0 to 18 deg). Spray angle error was measured by comparing the self-sensing feature of the piezoelectric stack actuator with results from an optical displacement sensor.

For each design, a hyperbolic tangent curve was fit to the CFD results with pintle position as the independent variable and spray angle as the dependent variable. Model validation involved conducting experimental spray tests using the second generation VGS prototype. The results in Fig. 5 show the differences in simulated and experimental spray angles, with an average absolute difference of 9.75 deg. However, both the mean spray angles (experimental: 72.35 deg, simulated: 74.34 deg) and spray ranges (experimental: 131.86 deg vs. simulated: 125.05 deg) correlated well enough to justify the use of CFD modeling for the design optimization process.

4 Formulating the Optimization Problem

Of the possible design parameters that fully define the 2-D model of the nozzle and pintle, six were chosen based on the results of preliminary CFD analyses. An optimization problem was formulated based on these six design parameters, $\vec{u}$, as shown in Fig. 6. Hard geometric constraints (Eq. (2)) were then formulated to reject infeasible injector geometries. An equality constraint was placed on the orifice diameter, u_6, to ensure adequate fuel droplet size

$$\begin{aligned}
&1000\,\mu\text{m} \le u_1 \le 2000\,\mu\text{m}\\
&400\,\mu\text{m} \le u_2 \le 800\,\mu\text{m}\\
&20\,\mu\text{m} \le u_3 \le 300\,\mu\text{m}\\
&140\,\text{deg} \le u_4 \le 180\,\text{deg}\\
&10\,\mu\text{m} \le u_5 \le 300\,\mu\text{m}\\
&u_3 + 2 \cdot u_2 \le u_1\\
&u_6 = u_1 + 200\,\mu\text{m}
\end{aligned} \tag{2}$$

4.1 Defining the Multiobjective Optimization Problem. Two competing objective functions were considered: actuator stroke (F_1) and spray angle sensitivity (F_2). The required stroke is directly proportional to the size and cost of the actuator, which should ideally be as small as possible. Spray angle sensitivity, defined as the maximum change in spray angle with respect to pintle position, represents the control challenge as sensitivity is directly proportional to errors in spray angle. Therefore, minimizing actuator stroke and spray angle gain reduces actuator cost and enhances the performance of the control system.

4.1.1 Actuator Stroke. The translational motion of the pintle must be actuated at speeds up to about 188 Hz [13], and the actuator must be capable of running continuously in an engine environment with minimal power consumption. For these reasons, a piezoelectric stack actuator was chosen. Because PZT stack

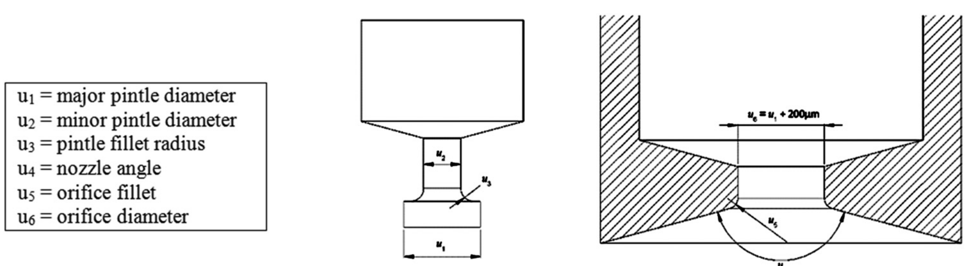

Fig. 6 The six VGS design variables for the nozzle (left) and pintle (right)

actuators have limited strain capabilities (approximately 0.1% [18]), a 10 cm long PZT stack was required for direct actuation with a 100 μm pintle stroke—much too large for practical implementation in an engine environment. Flexure mechanisms could be used to provide mechanical advantage and reduce actuator size. The actuator stroke objective function, F_1, is defined by

$$F_1 = x_{150} - x_{70} \tag{3}$$

Here, x_{150} is the pintle position when the spray angle is 150 deg and x_{70} is the pintle position when the spray angle is 70 deg. If a candidate design did not achieve the desired range of spray angles, its objective function was given a penalty proportional to the difference between the desired and achieved range.

4.1.2 Spray Angle Sensitivity. Spray angle sensitivity (G_{SA}) quantifies the change in spray angle ($d\theta$) with respect to pintle position (dPP), as shown as

$$G_{SA} = \frac{d\theta}{dPP} \tag{4}$$

Tracking errors in pintle position (e_{PP}) produce tracking errors in spray angle (e_{SA}) via the spray angle sensitivity

$$e_{SA} = e_{PP} \cdot G_{SA} \tag{5}$$

Because errors in pintle positioning are inevitable, it is important to minimize spray angle sensitivity. The sensitivity performance objective (F_2) is given by Eq. (6), where θ_i is the spray angle corresponding to the i th pintle position $y_{p,i}$ and n equals 9

$$F_2 = \max\left\{ i = 2, 3, \ldots, n \middle| \frac{\theta_i - \theta_{i-1}}{y_{p,i} - y_{p,i-1}} \right\} \tag{6}$$

Constraints were also placed on the objective functions to ensure reasonable performance values. For example, experimental testing with the second generation VGS prototype revealed that peak pintle position errors rarely exceeded 5 μm [8], so the maximum spray angle sensitivity was set to 1.5 deg/μm (corresponding to a peak spray angle error of 7.5 deg). The performance objective constraints used in this work are given as

$$\begin{aligned} F_1 &\leq 2000\,\mu\text{m} \\ F_2 &\leq 1.5\,\text{deg}\,/\mu\text{m} \end{aligned} \tag{7}$$

The multiobjective genetic algorithm (MOGA) in the Matlab Global Optimization Toolbox [19] was used to optimize system performance. Beyond the default settings, a randomly generated population of 50 was chosen and arithmetic crossover was selected with a crossover fraction of 0.80. Genetic algorithms were chosen for this work because they do not require gradient information and have been applied to a number of interesting design optimization problems [20–23].

4.2 Parallelizing Design Candidate Evaluation. To improve computational performance, a blade cluster at North Carolina State University's High-Performance Computing (HPC) group was used to evaluate up to 20 VGS designs simultaneously. The

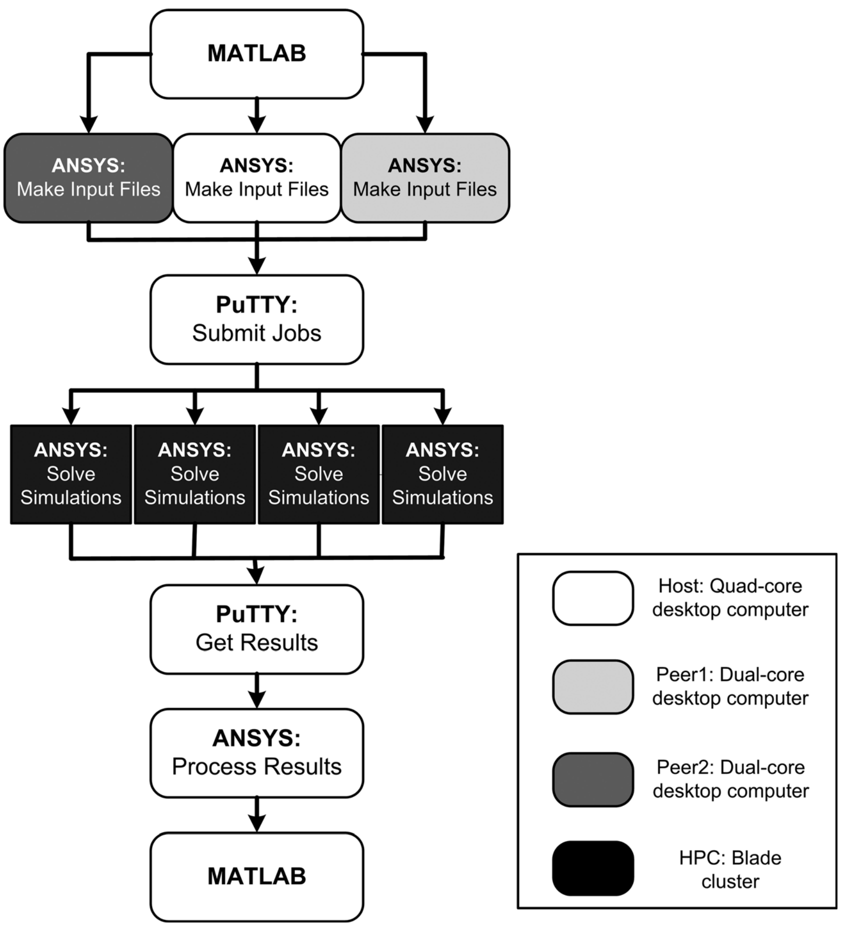

Fig. 7 Flow chart for the design evaluation process using the HPC (colors indicate which system performed each task)

Table 1 Variable bounds for three-point full-factorial study

Variable	Lower bound	Midpoint	Upper bound
u_1	1000 μm	1500 μm	2000 μm
u_2	400 μm	600 μm	800 μm
u_3	10 μm	150 μm	300 μm
u_4	140 deg	160 deg	180 deg
u_5	5 μm	150 μm	300 μm

freeware scripting engine AutoIt was used to automate communication between MATLAB, ANSYS, and the HPC, as shown in Fig. 7. The Autoit applications were designed to parallelize tasks as much as possible and to guard against a variety of timing issues and errors.

The goal of building this computer simulation framework was to facilitate design space exploration and find VGS geometries capable of performances that dominated existing prototype configurations. Results and analysis of from this simulation are presented in Sec. 5.

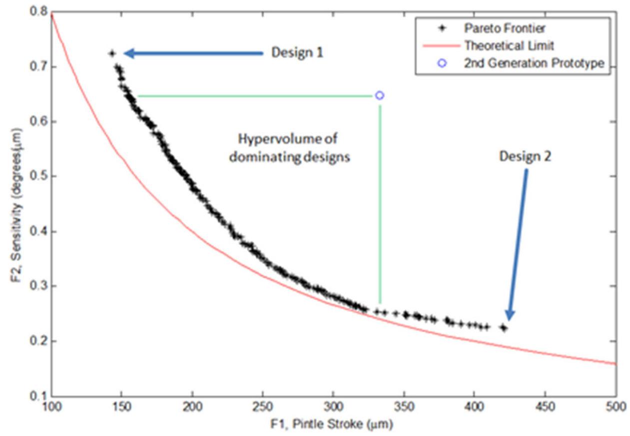

Fig. 10 VGS performance space highlighting the final Pareto frontier and the second generation prototype

5 Analysis of Results

This section reports and analyzes two different sets of results. Section 5.1 discusses the insights gained from a statistical analysis of the design to performance space relationship. The second subsection explores the results and lessons learned from evaluating the nondominated solutions obtained from the MOGA.

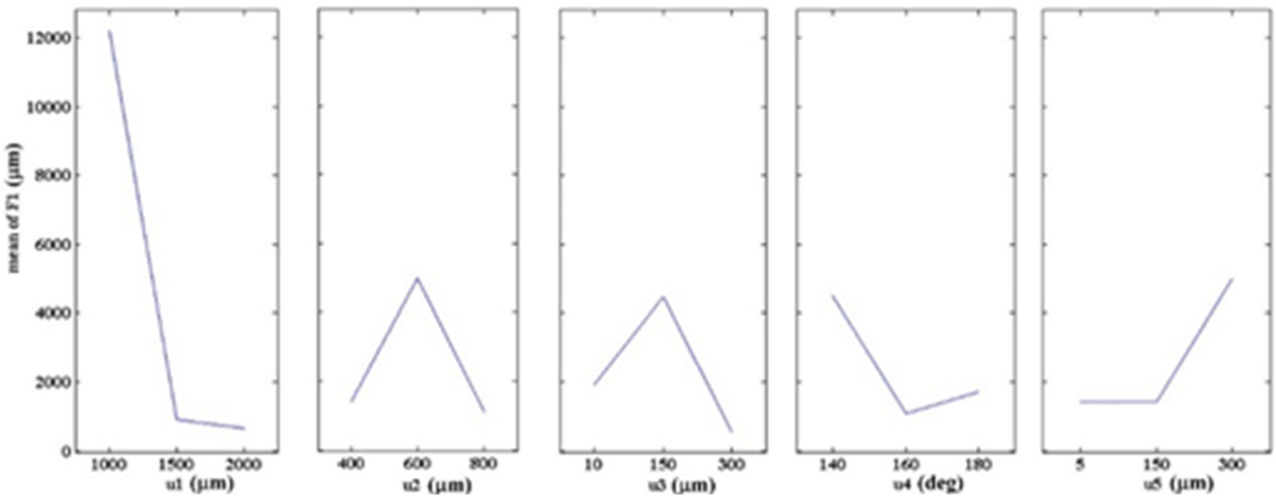

Fig. 8 Main effects plot for objective function *F*1

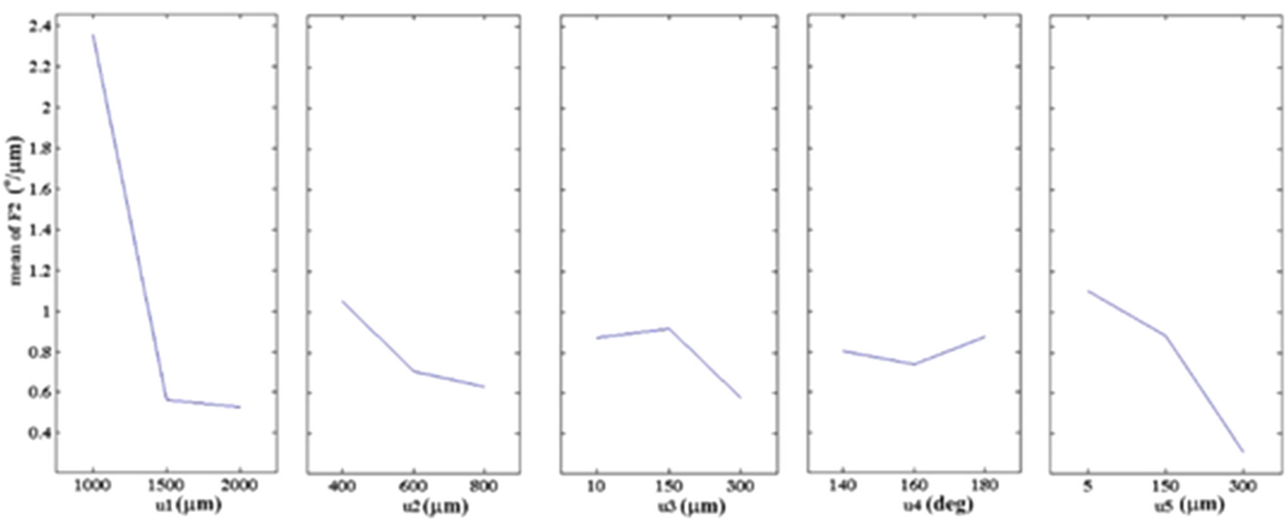

Fig. 9 Main effects plot for objective function *F*2

Table 2 Optimized design parameters and objective function values

Design	Objective functions F_1 (μm)	F_2 (deg/μm)	Design parameters Major pintle diameter u_1 (mm)	Minor pintle diameter u_2 (mm)	Pintle fillet u_3 (mm)	Nozzle angle u_4 (°)	Orifice fillet u_5 (mm)	Orifice diameter u_6 (mm)
Prototype 2	340.6	0.6472	1.500	0.729	0.254	150	0.000	1.700
Design 1	143.3	0.7242	1.972	0.612	0.278	160.57	0.019	2.172
Design 2	421.2	0.2228	1.632	0.640	0.104	172.15	0.300	1.832

5.1 Exploring the Design Space to Performance Space Relationship. A three-point full factorial was generated for the first five design variables, as shown in Table 1. Recall from Eq. (2) that the sixth design variable is part of an equality constraint and can be removed from the overall problem formulation. Evaluating this data set led to 168 feasible, converged designs.

A main-effects analysis was first conducted, as shown in Figs. 8 and 9. Both figures indicate that greater values of u_1, u_2, and u_3 are better for both objective functions. For u_4, the middle setting is the best for both objectives. Finally, u_5 presents a tradeoff: a larger value is better for F_2, but a smaller value is better for F_1.

A part-worth coefficient estimate of the different variable levels revealed a number of design variables that did not statistically influence the mean value of the objective function. To further explore this, a main-effects linear regression was estimated using

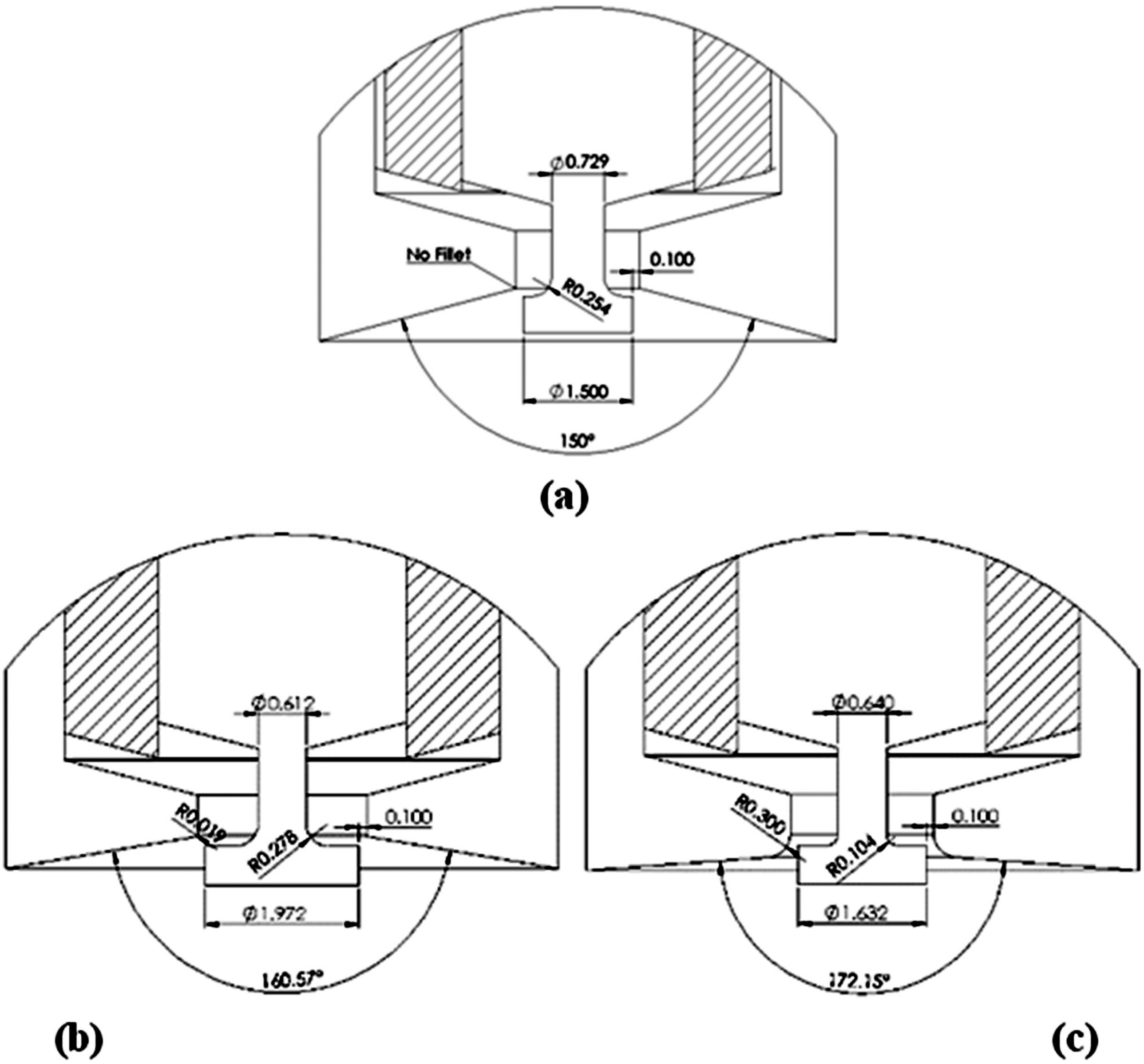

Fig. 11 The design variables (VGS geometries) for (*a*) the second generation prototype, (*b*) Design 1, and (*c*) Design 2

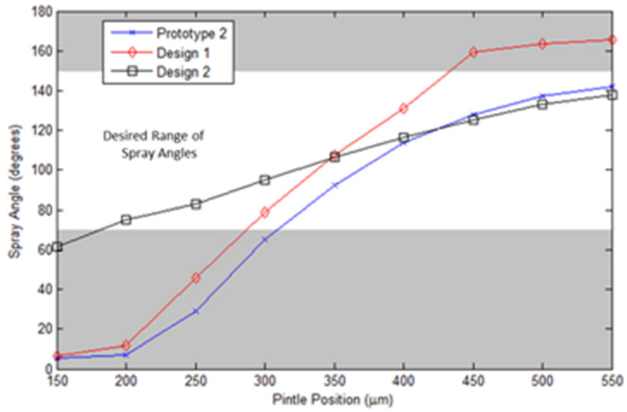

Fig. 12 Graph of spray angle versus pintle position for Design 1, Design 2, and the second generation prototype (Prototype 2)

a −1, 0, 1 data structure. From this fit, it was concluded that design variables u_1 ($p < 0.02$, $p < 0.001$), u_2 ($p < 0.86$, $p < 0.12$), and u_5 ($p < 0.21$, $p < 0.001$) were the only variables that statistically influenced either objective function. A full quadratic model was also estimated to determine if there were any significant second order effects.

Result analysis of the different regressions indicated that u_1 was the main driver of system performance (larger is better for both objectives). Variable u_2 had a main effect influence on F_2 but was only significant in higher order terms for objective F_1. Variable u_3 appeared to only influence F_1, while variable u_4 only impacted F_2 when interacting with other variables. Finally, u_5 posed a tradeoff between objectives, while its coefficient played a larger role in objective F_2.

5.2 Analyzing the MOGA Results. Having explored basic design variable effects, Fig. 10 shows the final MOGA results after 100 generations (20 days of analysis using HPC) in comparison to the performance of the second generation prototype. This optimization was computationally expensive because each design candidate required nine CFD calculations, as discussed in Sec. 3. Therefore, 5000 evaluated candidates required 45,000 CFD simulations to characterize how the spray angle changed with respect to pintle position. Convergence with respect to theoretical performance limits is also shown. These theoretical limits were found by calculating the best possible stroke for each value of spray angle sensitivity. For any given pintle stroke, the best spray angle sensitivity is that of a straight line, where the slope is constant. Therefore, the theoretical performance limit is defined by

$$F_2 = G_{SA} = \frac{\Delta\theta}{\Delta PP} = \frac{150\,\text{deg} - 70\,\text{deg}}{F_1} \tag{8}$$

The lines extending from the second generation prototype help depict the hypervolume of dominating designs [24, 25] found by the MOGA. The two extreme designs of the Pareto frontier are labeled Design 1 (shortest pintle stroke) and Design 2 (smallest spray angle sensitivity). The design and performance characteristics of Design 1, Design 2, and the second generation prototype are listed in Table 2 and Fig. 11.

The dependencies of spray angle on pintle position for these three designs were also examined, as shown in Fig. 12. Design 2 had a much smaller slope (sensitivity) than Design 1 but had a much greater actuator stroke. Further, while the spray angles were nonlinear with respect to pintle position for all three designs, nonlinearities in Design 1 and Design 2 were greatly reduced within the desired range of spray angles (70–150 deg). It is also important to note that Design 2 did not reach the full desired range of spray angles within the pintle range evaluated. However, the behavior of the data suggests that it will reach the desired spray angle of 150 deg as the pintle moves past 550 μm.

The scatter plot matrix shown in Fig. 13 depicts the relationship that exists between the design variables and each objective function. This data show that design tradeoffs must be made when design variables u_1, u_3, u_4, and u_5 are considered in the context for the two competing performance objectives. Design variable u_5, for example, demonstrates a clear conflict—an increase in u_5 provides a performance loss in F_1 but a performance gain in F_2. Design variable u_1 is interesting in that the performance loss associated with objective F_2 does not appear to be significant until the variable approaches the limit of the upper bound. This behavior could potentially provide a designer with a degree of design freedom, in that the "insensitivity" of F_2 to small changes in u_1 gives an opportunity to make a tradeoff without accepting a significant performance loss. Further, while the plots for design variable u_4 suggest that there is a slight tradeoff between objectives, there is no discernible trend for design variable u_2. However, for values of this variable at 0.5 mm and larger, the performance of the system can vary significantly.

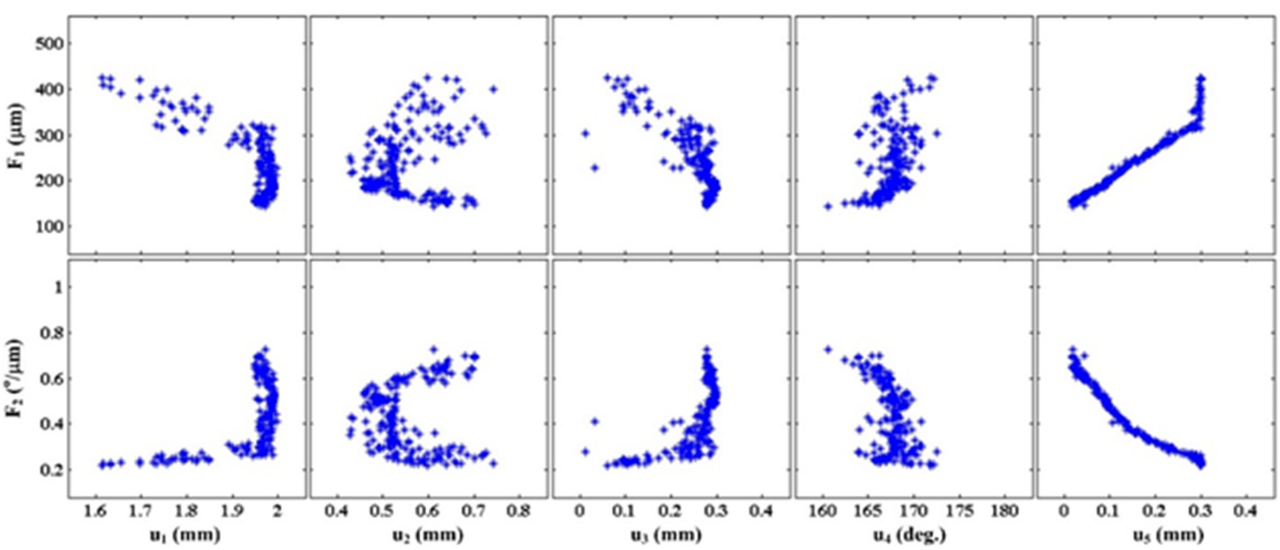

Fig. 13 Scatter plot matrix of design variable values on Pareto frontier

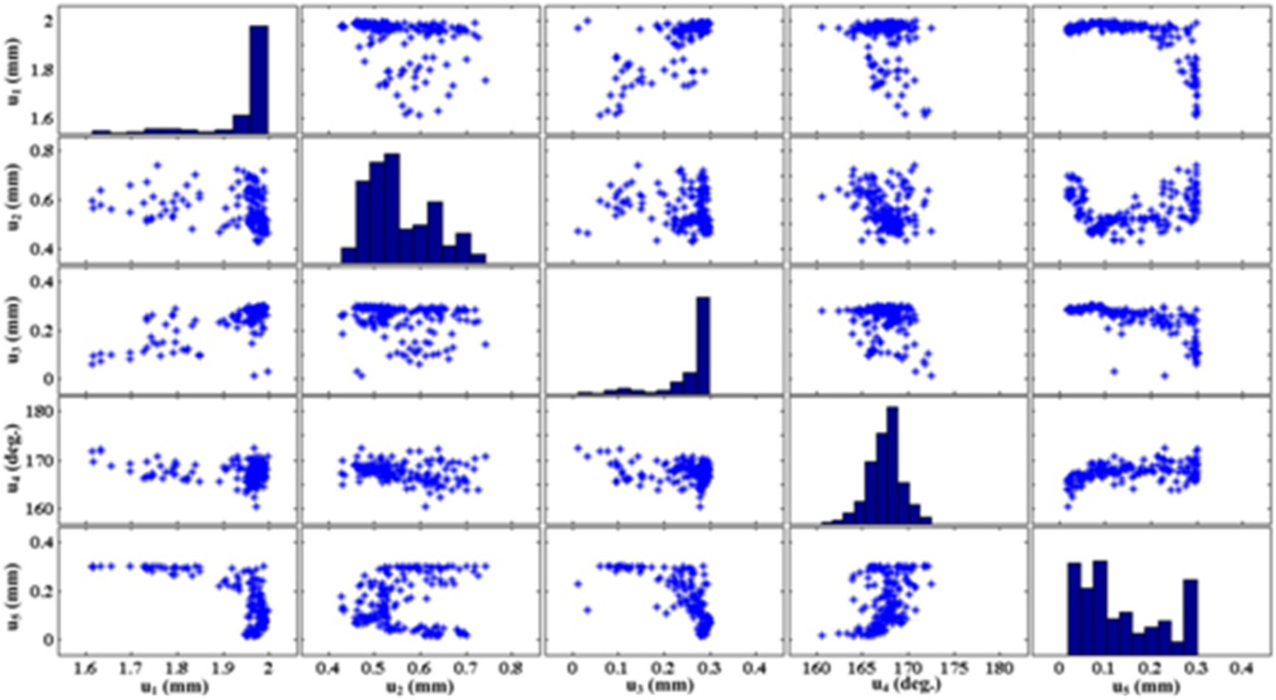

Fig. 14 Scatter plot matrix of design variable relationships

Relationships in design variable behavior are highlighted in Fig. 14. Here, design variables u_1 and u_3 are primarily at the upper regions of their allowable ranges. Some variables, like u_2 and u_5, are more distributed. Finally, the data in this figure suggest that there are noticeable interactions between design variables u_1 and u_5, u_2 and u_5, and u_3 and u_5. For instance, until u_5 is at its upper bound, u_1 on the frontier is at its upper bound.

6 Conclusions

This paper interfaced a MOGA with CFD analysis software to evaluate candidate VGS designs. The CFD model was validated by comparison to empirically measured spray test results from prior prototypes. Due to the high computational cost to evaluate candidate designs, a HPC cluster was employed to evaluate as many as 20 designs at once. The MOGA found a Pareto frontier with significant opportunity for performance improvements over a prior prototype. Further, by examining two design cases at the extremes of the Pareto frontier, critical relationships between the design parameters and the performance objectives were identified.

Future work should focus on the fabrication and testing of extreme Pareto designs (Design 1 and Design 2) to verify the optimization results and demonstrate the improved control and actuation of the injector. Additional work could integrate a more powerful CFD tool, such as KIVA, to predict fuel flows, air flows, and ignition and combustion processes [26]. Using KIVA, the droplet size constraints could be computationally evaluated, adding an additional degree of freedom to the design space by removing the need for a geometric equality constraint. Finally, the optimization could be run with additional performance objectives such as droplet size, combustion performance, and material cost to investigate other important design considerations.

Acknowledgment

This research was supported in part by the National Science Foundation under Grant Nos. CBET-0854174 and CMMI-1054208. Any opinions, findings, and conclusions or recommendations expressed in this material are those of the author(s) and do not necessarily reflect the views of the funding agencies.

References

[1] *Federal Register*, 66:5002–5193, 2001.
[2] Yao, M., Zheng, Z., and Liu, H., 2009, "Progress and Recent Trends in Homogeneous Charge Compression Ignition (HCCI) Engines," Prog. Energy Combust. Sci., 35(5), pp. 398–437.
[3] Christensen, M., 2002, "HCCI Combustion-Engine Operation and Emission Characteristics," Ph.D. thesis, Department of Heat and Power Engineering, Lund University, Lund, Sweden.
[4] Gatellier, B., Walter, B., and Miche, M., 2001, "New Diesel Combustion Process to Achieve Near Zero NO_x and Particulates Emissions," *A new generation of engine combustion processes for the future?*, Technip, Paris, pp. 43–52.
[5] Duffy, K., 2004, "Heavy Truck Clean Diesel (HTCD) Program," *Diesel Engine Emission Reduction Conference*, Coronado, CA.
[6] Sun, Y., and Reitz, R., 2006, "Modeling Diesel Engine NOx and Soot Reduction with Optimized Two-Stage Combustion," *SAE 2006 World Congress & Exhibition* Warrendale, PA, SAE Paper No. 2006-01-0027.
[7] Fang, T., Coverdill, R., Lee, C., and White, R., 2008, "Effects of Injection Angles on Combustion Processes Using Multiple Injection Strategies in an HSDI Diesel Engine," Fuel, 87(15–16), pp. 3232–3239.
[8] Lien, J., 2011, "Design, Modeling, and Control of a Variable Geometry Spray Fuel Injector," Ph.D. thesis, Department of Mechanical and Aerospace Engineering, North Carolina State University, Raleigh, NC.
[9] Niebrzydoski, J., 1995, "Fuel Injection System for Internal Combustion Engines," U.S. Patent 5,398,654.
[10] Ferguson, S., Lewis, K., Siddiqi, A., and de Weck, O., 2007, "Flexible and Reconfigurable Systems: Nomenclature and Review," *ASME Design Engineering Technical Conferences*, *Design Automation Conference*, Las Vegas, NV, Paper No. DETC2007/DAC-35745.
[11] Lien, J., Zhang, J., Fang, T., and Buckner, G., 2011, "Preliminary Testing of Sprays With Continuously Variable Spray Geometry," *Proceedings of the ILASS-Americas 23rd Annual Conference on Liquid Atomization and Spray Systems*, Ventura, CA.
[12] Kastengren, A. L., Tilocco, F. Z., Powell, C. F., Manin, J., Pickett, L. M., Payri, R., and Bazyn, T., 2012, "Engine Combustion Network (ECN): Measurements of Nozzle Diameter and Hydraulic Behavior of Diesel Sprays," Atomization and Sprays.
[13] Archer, J., Lien, J., Fang, T., and Buckner, G., 2012, "Close Loop Control of Continuously Variable Geometry Sprays," *Proceedings of the ILASS-Americas 24th Annual Conference on Liquid Atomization and Spray Systems*, San Antonio, TX.
[14] Fujii, H., 2007, "Injector for High-Pressure Injection," U.S. Patent 7,222,608.

[15] ANSYS, Inc. ANSYS Workbench 12.0, Canonsburg, PA, 2008.
[16] Python Software Foundation, Python 2.7.5, http://www.python.org
[17] Date, A., 2005, *Introduction to Computational Fluid Dynamics*, Cambridge University Press, New York, Chap. 6.
[18] Suleman, A., Prasad, E., Blackow, R., and Waechter, D., 2001, "Smart Structres—An Overview," *Smart Structures: Applications and Related Technologies*, A. Suleman, ed., Number 429 in CISM Courses and Lectures, Springer, Italy, pp. 3–16.
[19] The Mathworks, Inc., 2013, *Matlab version 2013a, Global Optimization Toolbox*, Natick, MA.
[20] Kudikala, R., Kalyanmoy, D., and Bhattacharya, B., 2009, "Multi-Objective Optimization of Piezoelectric Actuator Placement for Shape Control of Plates Using Genetic Algorithms," ASME J. Mech. Des., **131**(9), p. 091007.
[21] Deb, K., and Jain, S., 2003, "Mutli-Speed Gearbox Design Using Multi-Objective Evolutionary Algorithms," ASME J. Mech. Des., **125**(3), pp. 609–619.
[22] Shahi, S., Wang, G., An, L., Bibeau, E., and Pirmoradi, Z., 2011, "Using the Pareto Set Pursuing Multiobjective Optimization Approach for Hybridization of a Plug-In Hybrid Electric Vehicle," ASME J. Mech. Des., 133(9), p. 094503.
[23] Zhang, X., and Nelson, C., 2011, "Multiple-Criteria Kinematic Optimization for the Design of Spherical Serial Mechanisms Using Genetic Algorithms," ASME J. Mech. Des., **133**(1), p. 011005.
[24] Beume, N., Naujoks, B., and Emmerich, M., 2007, "SMS-EMOA: Multiobjective Selection Based on Dominated Hypervolume," Eur. J. Oper. Res., **181**(3), pp. 1653–1669.
[25] Wu, J., and Azarm, S., 2001, "Metrics for Quality Assessment of a Multiobjective Design Optimization Solution Set," ASME J. Mech. Des., **123**(1), pp. 18–25.
[26] Los Alamos National Laboratory, 2010, KIVA, Los Alamos, NM.